Improvement of Surface Accuracy for High-Precision Space Antenna by Design Optimization of Adaptive Structure System

Improvement of Surface Accuracy for High-Precision Space Antenna by Design Optimization of Adaptive Structure System

By Yasutaka Satou[1)], Hiroshi Furuya[1)], and Nozomu Kogiso[2)]

[1)]*Department of Built Environment, Tokyo Institute of Technology, Yokohama, Japan*
[2)]*Department of Aerospace Engineering, Osaka Prefecture University, Osaka, Japan*

This paper addresses the design of a high precision space antenna with the adaptive structure system by simultaneous optimization of the structure and the actuators. The results of the design optimization show that the higher precision surface can be obtained by the simultaneous optimum design than the individual optimum design of the actuators. The feasibility of the simultaneous optimum design is examined experimentally. The surface error obtained by the experiment is in agreement with the surface error of the design optimization, and thus, the feasibility of the simultaneous optimum design is verified.

Key Words: Simultaneous Optimization, Surface Accuracy, Optimum Design

1. Introduction

High precision space antennas, such as Muses-B[1)] and Astro-G[2)], have the subject of continued interest and developed in the past several decades. The required surface accuracy for the space antenna have become higher and higher to realize the high radio frequency survey. In the space environment, the surface accuracy can be degraded easily due to the disturbances, such as the aging degradation of the material and the thermal deformation. Thus, the antenna system, which can maintain the surface accuracy in the space environment, is requested.

The adaptive structure system[3)] is one of the systems to maintain the surface accuracy of the space antenna. The adaptive structure system controls and corrects the structure by using the actuators to adapt the space environment. When the adaptive structure system is introduced to the structure, the performance of the shape correction is determined by the stiffness distribution of the structure and the output force and the location of the actuator. However, in the conventional study, the structure and the actuator are treated individually, especially for the actuators[4,5)]. Therefore, it is significant to design the structure and the actuators simultaneously.

In this paper, the design of the high precision space antenna with the adaptive structure system is examined by the simultaneous optimization of the structure and the actuators to improve the surface accuracy. At first, the simultaneous optimization of structure and actuators is performed. Then, the feasibility of the optimum design is verified experimentally. Finally, the optimum design is discussed based on the results of the design optimization and the experiment.

2. Analysis Model of Rib-Stiffened Shell Antenna

This section presents the design domain and the analysis model of the space antenna.

2.1. Overview of rib-stiffened shell antenna

Several conventional antenna structures have been developed, such as the membrane, the mesh, the solid, and the shell. The membrane and the mesh antenna are difficult to realize the high precision surface because these antennas approximate the parabolic surface by polyhedron. In the case of the solid antenna, the parabolic surface can be realized, and the surface shape can be controlled by fewer actuators because the deformation by the actuators becomes global due to the high stiffness. However, the higher stiffness requests the higher output force of the actuator to control the surface shape, and hence, when the output force is limited, the shape control becomes difficult. On the other hand, the shell antenna can form the parabolic surface and can deform easily by the actuators. When the ribs are attached to the shell surface, the deformation becomes global, and the shape control can be realized by fewer actuators. In this paper, therefore, the rib-stiffened shell antenna is treated as shown in Fig.1. In consideration of the rotation symmetry of the antenna, the selected area in Fig.1 is treated as the design domain.

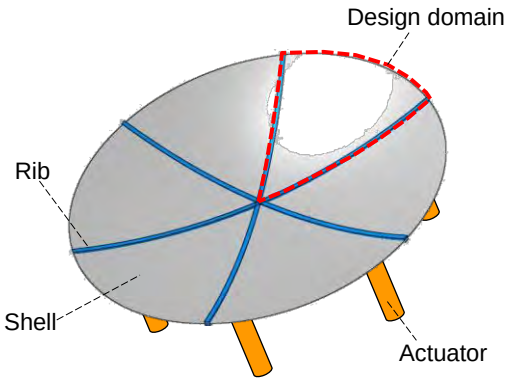

Fig. 1. Overview of rib-stiffened shell antenna

2.2. Analysis model of rib-stiffened shell antenna

Figure 2 shows the analysis model of rib-stiffened shell antenna. In the model, the asymmetric deformation mode cannot be treated because the rotation symmetry is assumed. The nominal configuration of the analysis model is the ideal parabolic surface, where the focal length is 500mm. The configuration of the analysis model projected on the r-θ plane is an equilateral triangle whose one side is 500mm. In Fig.2, x, r, and θ are global coordinate, x_r, y_r, and z_r are rib fixed coordinate. The configuration of rib is a cylindrical shape whose diameter is $d(x_r)$. The thickness of the shell is $t(r)$. The material constants of the rib and the shell are indicated in Table 1. The location of the actuator is $x_r = x_F$, where the attachment angle and the output force are θ_F and F, respectively. The boundary conditions of the analysis model are shown as follows.

1. Rib is cramped at $(x, r) = (0, 0)$
2. Deformation of rib is symmetry with respect to y_r

The nominal design of the rib-stiffened shell antenna is as follows.

- $d(x_r) = 10$mm
- $t(r) = 0.5$mm
- $x_F = 250$mm
- $F = 5.0$N
- $\theta_F = 0.7$

Table 1. Material constant

	Rib	Shell
Young's modulus [GPa]	132	70
Poisson's ratio	0.3	0.3
Density [ton/mm^3]	8.75e-9	2.40e-9
Thermal expansion coefficient [1/K]	1.76e-5	2.30e-5

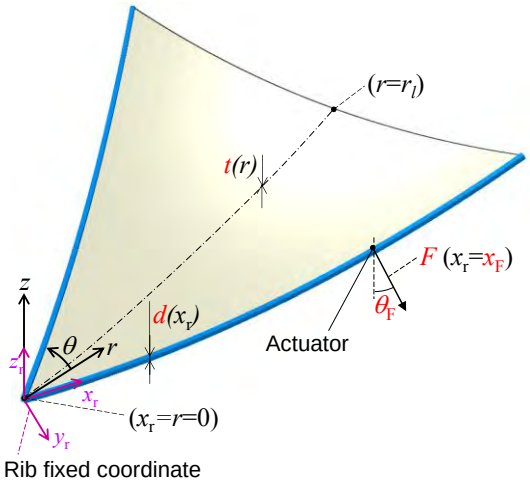

Fig. 2. Analysis model of rib-stiffened shell antenna

3. Design Optimization Method

In the design optimization, the root mean square (RMS) of the surface error, where the disturbance and the output force of the actuator are applied, is minimized. The details of the design optimization are presented in this section.

3.1. Objective function

The objective function is the root mean square of the surface error so as to improve the surface accuracy. The surface error is evaluated in consideration of the electric field intensity of the aperture. Simple tapered pattern[6,7], which is one of the typical electric field intensity as shown in Eq.(1), is employed.

$$A = A_0 \cdot 10^{[A_x(\theta/\theta_0)^2/20]} \tag{1}$$

where θ is the angle between the boresight direction and the direction from the point on the surface, θ_0 is the angle between the boresight direction and the direction from the edge of the surface, A_x is the amplitude level at $\theta=\theta_0$ relative to the maximum level, and A_0 is a normalization constant. Although the value of A_x has to be determined in consideration of the antenna model in the practical design, in this paper, the value is assumed to be -10dB as the general case. The electric field intensity Eq.(1) is introduced as the weighting function of the surface error as,

$$\varepsilon_{rms} = \sqrt{\frac{\sum_{i=1}^{N} A_i \varepsilon_i^2}{\sum_{i=1}^{N} A_i}} \tag{2}$$

where $\varepsilon_{\mathrm{rms}}$ is the root mean square of the best fit surface error considering the electric field intensity, A_i is electric intensity at node i, ε_i is the surface error at node i, and N is the number of the node.

3.2. Optimization program

The design optimization is carried out by VisualDOC[8]. The VisualDOC can integrate with several commercial analysis programs. The optimization algorithm, which is employed in the design optimization, is Particle Swarm Optimization (PSO)[8]. PSO uses probabilistic search directions and works with a set of solutions. The PSO emulates the social behavior of a group of birds or fish moving together. The information of the current best solution in the group is exchanged in the group, and the own best velocity and position are updated based on the best solution in the group. The PSO is employed because of the following two points. The first point is the optimization problem has many design variables. The second point is the solution depends on the initial condition of the optimization.

3.3. Finite element analysis program

The structural analysis is performed by the finite element analysis program ABAQUS[9]. In the FEA, the analysis procedure is static and linear, where the deformation of the antenna is assumed to be sufficiently smaller than the antenna size. The rib and the shell is modeled by the beam elements and the shell elements, respectively.

3.4. Design optimization process

The flowchart of the design optimization process is indicated in Fig.3. The optimization is carried out by the following process.

1. Read original finite element model
2. Define design variables and generate ABAQUS input

file
3. Apply disturbance and analyze the deformation
4. Analyze the deformed configuration after shape correction
5. Calculate surface error and optimize the design variables

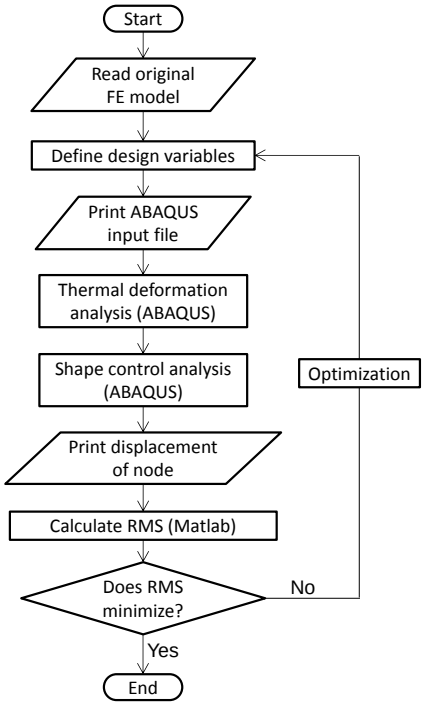

Fig. 3. Flowchart of design optimization process

4. Design Optimization of Rib-stiffened Shell Antenna

This section presents an example of the design optimization of rib-stiffened shell antenna. To verify the effectiveness of the simultaneous optimum design, the individual optimum design of the actuators is also investigated as the contrast analysis. The design variables and the constraints are as follows.

- Design variables
  - $d(x_r)$, Distribution of rib thickness (9 points are optimized and interpolated)
  - $t(r)$, Distribution of shell thickness (9 points are optimized and interpolated)
  - x_F, Location of actuator
  - F, Output force of actuator
  - θ_F, Angle of actuator
- Constraints
  - Mass of antenna < 1000g
  - 2.0mm < $d(x_r)$ < 20mm
  - 0.1mm < $t(r)$ < 1.0mm
  - 0.0N < F < 50N
  - $-\pi/2 < \theta_F < \pi/2$

Figure 4 shows the deformed configuration when the disturbance is applied to the nominal design, where the output force of the actuator is not applied. The disturbance is the thermal deformation. The temperature around the center of the antenna is high (T_C=0[ºC]) and the temperature around the edge of the antenna is low (T_E=-200[ºC]). In addition, we assume the linear temperature gradient as,

$$\Delta t = \frac{T_E - T_C}{r_1} \times r \tag{3}$$

As the temperature around the antenna edge is lower than the temperature of the center, the thermal strain around the edge becomes negative, and hence, the edge of the antenna shrinks. As the boundary condition of the antenna model considers the rotation symmetry indicated by the boundary condition 2 in Section 2.2, the antenna surface deforms upper side as shown in Fig.4.

The configurations, where the output force of the actuator is applied and the shape correction is carried out, are indicated in Fig.5a and b. Fig.5a shows the results of the individual optimum design of the actuators. In the individual design, the location, the angle, and the output force of the actuator are optimized, and the design variables of the structure are nominal design. On the other hand, Fig.5b shows the results of the simultaneous optimum design, where the design variables of the structure and the control system are optimized. In these figures, the counter plot shows the out-of-plane deformation of the antenna surface. Table 2 shows the results of the optimization.

In the individual optimum design, as shown in Fig.5a, the edge of the surface waves. The wave is induced by the circumferential constraint. As shown in Table.2, the angle of the actuator is -76.3[deg] and the location of the actuator is on the edge of the rib, and hence, the edge of the antenna is displaced in the inner direction. In that case, the compressive stress in the circumferential direction is applied to the shell because the circumferential displacement of the antenna is constrained due to the boundary condition 2 indicated in Section 2.2. As the results, the edge of the antenna waves. When the wave is induced in the shell surface, the surface error becomes large. Thus, it is significant to design the antenna structure and the actuator so as not to induce the wave.

In the simultaneous optimum design, as shown in Fig.5b, the wave, which is shown in the individual optimum design, is not observed. It is because the thickness of the rib and the shell are optimized. Figure 6a and b indicate the thickness distribution of the rib and the shell, respectively. As shown in the figures, the rib thickness around the edge is small. On the other hand, the shell thickness around the edge is large. In that case, the deformation of the shell is independent of the deformation of the rib. Thus, the wave can be avoided by the optimization of the structure. In addition, the location of the actuator is not on the edge of the rib, and the rib and shell thickness is small around the location of the actuator. In that case, the surface control becomes easier, and the output force becomes sufficient to improve the surface accuracy.

To evaluate the efficiency of the shape correction, control efficiency E is introduced in terms of the surface error before shape correction ε^B_{rms} and the surface error after the shape correction ε^A_{rms} as,

$$E = \frac{\varepsilon^B_{rms} - \varepsilon^A_{rms}}{\varepsilon^B_{rms}} \tag{4}$$

The control efficiencies of the results of the optimization are

indicated in Table.2. In the case of the individual optimum design of the actuators, the control efficiency is 20%. On the other hand, the control efficiency of the simultaneous optimum design is 53%. Hence, the control efficiency of the simultaneous optimum design is 2.65 times larger than that of the individual optimum design of actuators. Therefore, the higher precision surface can be realized by the simultaneous optimum design of structure and the actuators.

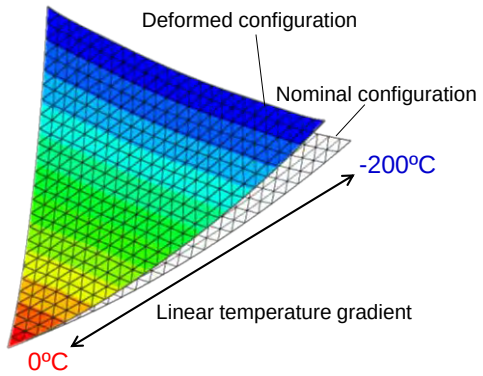

Fig. 4. Deformed configuration of nominal design under disturbance without shape correction

Table 2. Results of the design optimization

	Individual optimum design of actuators	Simultaneous optimum design
Surface error, ε_{RMS} [mmRMS]	0.524	0.307
Control efficiency, E [%]	20	53
Actuator location, x_F [mm]	500	180
Output force, F [N]	50.0	29.8
Angle of actuator [deg]	-76.3	-35.3

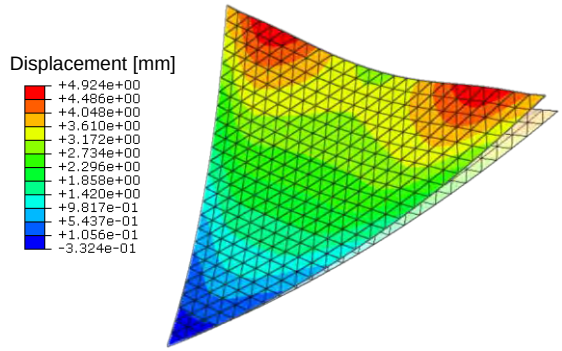

(a) Individual optimum design of actuators

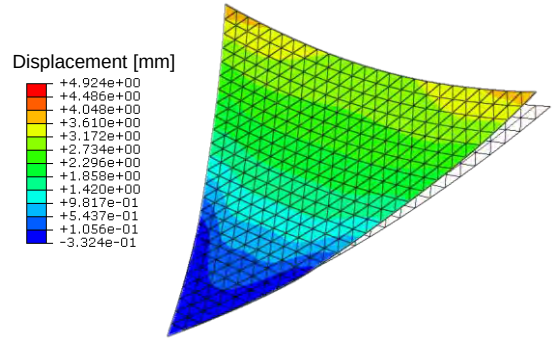

(b) Simultaneous optimum design

Fig. 5. Deformed configuration after shape correction

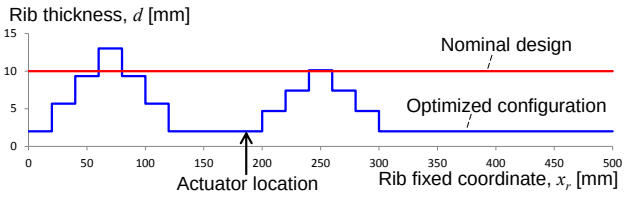

(a) Distribution of rib thickness

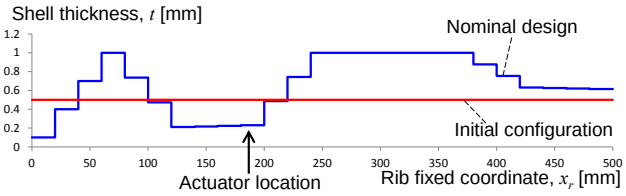

(b) Distribution of shell thickness

Fig. 6. Rib and shell distribution by simultaneous design optimization

5. Experimental Verification of Design Optimization

In this section, the feasibility of the simultaneous optimum design is verified by demonstrating experiments. In this study, as the preliminary experiment, we treat the flat rib-stiffened shell antenna, where we assume that the focal length is infinite. At first, the simultaneous optimum design of the structure and the actuators is investigated for the flat rib-stiffened shell antenna by using the design optimization method examined in Section 3. Then, the experimental specimen is manufactured based on the results of the design optimization, and the feasibility of the optimum design is examined.

5.1. Optimum design for flat rib-stiffened shell antenna

The optimum design of the flat rib-stiffened shell antenna is examined by using the design optimization method indicated in Section 3. Figure 7 shows the analysis model for the flat rib-stiffened shell antenna. The center of the antenna is constrained. On the other hand, the boundary condition 2, which is indicated in Section 2.2., is not considered to simplify the experimental setup. In addition, it is difficult to manufacture the shell which has the thickness distribution, and hence, the distribution of the shell thickness is not included in the design parameter of the optimization. The angle of the actuator is also difficult to setup. Based on the above description, the design variable and the constraints for the optimization are as follows.

- Design variables
  - $t_r(x_r)$, Distribution of rib thickness (4 points are optimized and interpolated)
  - x_F, Location of actuator
  - F, Output force of actuator
- Constraints
  - Mass of antenna < 1000g
  - 3.0mm < $t_r(x_r)$ < 10mm
  - 0.0N < F < 18N

The disturbance is the dead weight of the antenna specimen and the load on the rib described by yellow points indicated in

Fig.7. The other parameters are indicated in Table.3.

Figure 8 shows the distribution of the surface error obtained by the simultaneous design optimization. When the disturbance is applied to the antenna, the surface error is 1.09mmRMS. On the other hand, the surface error after the shape correction is 0.218mmRMS. As the surface error becomes 0.2 times by the shape correction, the effectiveness of the adaptive structure system is verified numerically for the flat rib-stiffened shell antenna. The rib configuration obtained by the optimization is indicated in Fig.9. Additionally, the optimum location of the actuator is x_F=320mm and the optimum output force of the actuator is F=8.6N. These optimal parameters are used in the experiments.

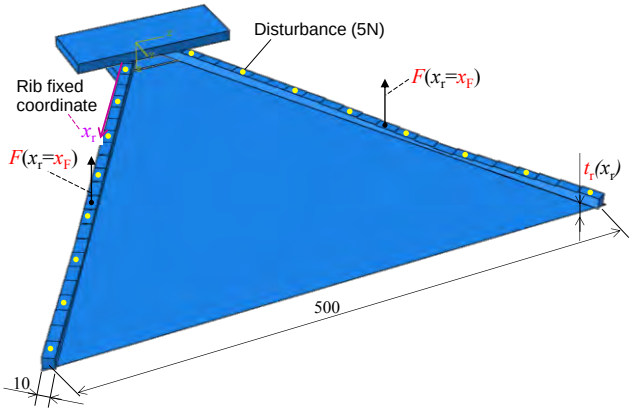

Fig. 7. Analysis model of flat rib-stiffened shell antenna

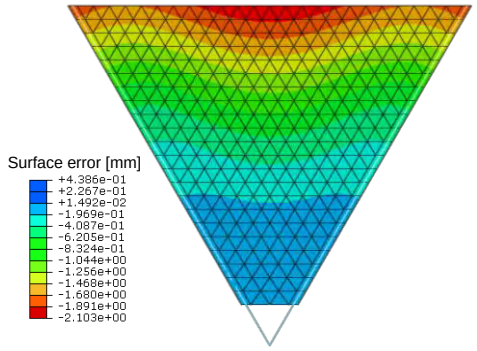

(a) Before shape control

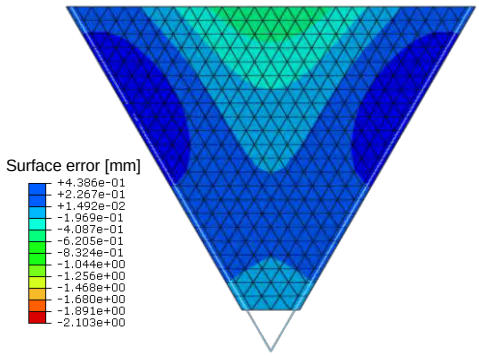

(b) After shape control

Fig. 8. Distribution of surface error

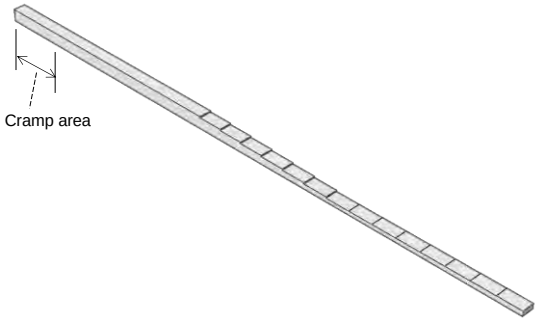

Fig. 9. Rib configuration obtained by optimization

Table 3. Parameters for flat rib-stiffened shell antenna

Young's modulus [GPa]	70
Poisson's ratio	0.3
Density [ton/mm^3]	2.7e-9

5.2. Experimental setup

The overview of the experimental setup is indicated in Fig.10. The antenna specimen is manufactured by attaching the rib to the 0.5mm flat-triangular shell. The optimized rib is manufactured by machine work. The material of the shell and the rib are aluminum. For the actuator, the tensile force is applied to the rib by nylon cable. The value of the tensile force is adjusted by tuning the length of the cable, where the value is measured by the load cell. The disturbance is applied by loading weights on the rib. The deformed shape of the antenna surface is measured by a laser displacement meter attached on the XY stage. The experimental equipment is located on the surface plate supported by vibration isolators.

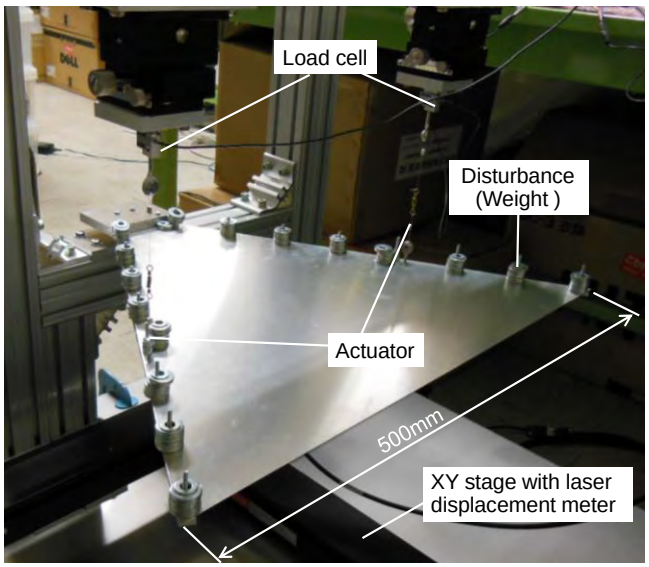

Fig. 10. Experimental setup

5.3. Experimental results

Table 4 shows the surface error obtained by the simulation and the experiments. When the antenna specimen is measured, the surface error before shape control and after shape control become 0.437mmRMS and 1.28mmRMS, respectively. These results are different from the numerical results qualitatively and quantitatively. The difference is caused by the misalignment of the attachment angle of the antenna specimen,

and hence, the XY stage and the antenna specimen are not parallel each other in the nominal configuration. To verify the above prediction, the configuration obtained by the experiment is corrected as,

$$w' = w_{Exp} - (w^0_{Exp} - w^0_{FEM}) \quad (5)$$

where w_{Exp} is the configuration after shape control obtained by the experiments, w^0_{Exp} is the configuration of the antenna specimen without disturbance and shape control, and w^0_{FEM} is the configuration of the analysis model without disturbance and shape control. In Eq.(5), w^0_{FEM} is used because the configuration without the dead load of the antenna specimen cannot be measured in the experiments. As shown in Table 4, the surface error with correction before shape control and after shape control become 1.10mmRMS and 0.149mmRMS, respectively. These values are in agreement with the surface error obtained by the simulation. Additionally, Fig.11 shows the distribution of surface error before shape control and the after shape control. These error distribution is qualitatively agreement with the error distribution obtained by simulation in Fig.8. Therefore, the feasibility of the simultaneous optimum design is verified. On the other hand, it is found that the misalignment of the setup affects the surface error, and the attachment accuracy of the antenna is significant to realize the high precision surface.

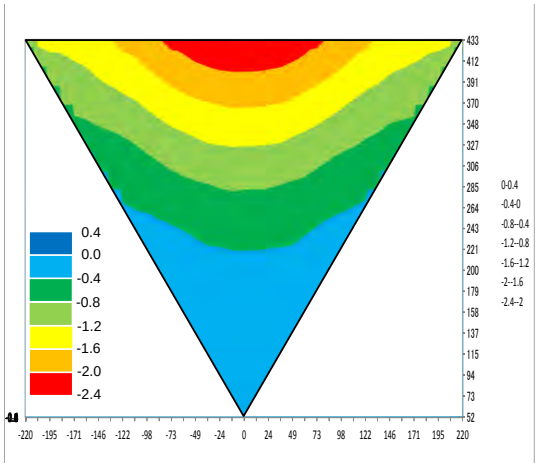

(a) After applying disturbance

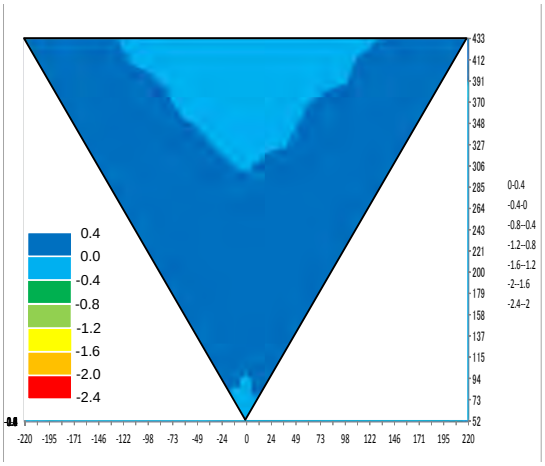

(b) After shape correction

Fig. 11. Distribution of surface error in experiments

Table 4. Surface error in simulation and experiments

	Before shape control	After shape control
Simulation	1.09mmRMS	0.218mmRMS
Exp.(w=w_{Exp}, without correction)	0.437mmRMS	1.28mmRMS
Exp.(w = w', with correction)	1.10mmRMS	0.149mmRMS

6. Conclusions

The simultaneous optimum design of the structure and the control system for the high precision rib-stiffened shell antenna was examined numerically and experimentally. The effectiveness of the simultaneous optimum design was verified because the surface accuracy of the simultaneous optimum design was higher than that of the individual optimum design of actuators. As the surface error obtained by experiments were agreement with the results of simulation, the feasibility of the optimum design was verified experimentally.

Acknowledgments

This work has been supported by JAXA's Strategic Research Grant and by JSPS KAKENHI Grant Number 24.10078.

References

1) Natori, M. C., Takano, T., Noda, T., Tashima, T., and Tabata, T.: Ground Adjustment Procedure of a Deployable High Accuracy Mesh Antenna for Space VLBI Mission, Proc., 39th AIAA/ASME /ASCE/AHS/ASC Structures, Structural Dynamics and Materials Conference, 1998, pp.1-11.
2) Natori, M. C., Hirabayashi, H., Okuizumi, N., Iikura, S. and Nakamura, K.: A Structure Concept of High Precision Mesh Antenna for Space VLBI Observation, Proc., 43rd AIAA/ASME /ASCE/AHS/ASC Structures, Structural Dynamics, and Materials Conference, 2002, pp.1-8.
3) Fang, H., Im, E., Quijano, U.O., Wang, K.W. , Hill, J., Moore, J., Pearson, J., Lui, C., Djuth, F.: High-Precision Adaptive Control of Large Reflector Surface. Proc., The 8th annual NASA Earth Science Technology Conference, 2008, pp.1-6.
4) Datashvili, L., Baier, H., Wei, B., Hoffman, J., Wehrle, E., Schreider, L., Mangenot, C., Santiago-Prowald, J., Scolamiero, L., Angevain, JC.: Mechanical Investigations of in-Space-Reconfigurable Reflecting Surfaces, Proc. ESA Antenna Workshop, 2010, pp.1-8.
5) Sasaki, K., Ishimura, K., and Tanaka, H.: Optimal Allocation of Actuators for Smart Reflector based on Modal Decomposition, Proc., 54th JSASS/JSME/JAXA Structures Conference, 2012, pp.215-217. (in Japanese)
6) Tanaka, H., Akita, T., Ishimura, K., and Sasaki, K.: Research on the gain variation caused by surface error of satellite-borne antenna, Proc. 27th Symposium on Aerospace Structure and Materials, 2011, pp.1-6. (in Japanese)
7) Pontoppidan, K.: Simple tapered pattern, GRASP9 Technical Description, TICRA Engineering Consultants, 2005, pp.109-110.
8) VisualDOC theory manual, Version 7.0, VANDERPLAATS RESEARCH & DEVELOPMENT Inc., 2011.
9) ABAQUS user's manual, Ver. 6.11, ABAQUS Inc., 2011.